Three-Dimensional Image Analysis of Single-Headed Heavy Meromyosin bound to Actin-Tropomyosin Filament

Hian Ann Ting

23th January, 1988

submitted to

Department of Physics, University of Tokyo

for the Degree of Master of Science

Thesis supervisor: Prof. Takeyuki Wakabayashi

Abbreviations

CBB: Coomassie Brilliant Blue

CyDTA: Trans-1,2-Cyclohexanediamine-N,N,N′,N′ -tetraacetic acid

HMM: heavy meromyosin

S1: myosin subfragment 1

LC1: myosin light chain-1

LC2: myosin light chain-2

LC3: myosin light chain-3

HC: heavy chain

HPLC: high performance liquid chromatography

DTT: dithiothreitol

DMF: N,N-dimethylformamide

DTNB: 5,5′-dithiobis(2-nitrobenzoic acid)

EDTA: ethylenediaminetetraacetic acid

PMSF: phenylmethanesulfonyl fluoride

SDS: sodium dodecyl sulphate

SDS-PAGE: SDS polyacrylamide gel electrophoresis

sHMM: single-headed Heavy Meromyosin

3-D: three-dimensional

TM: tropomyosin

Contents

Summary

Three-dimensional structure of actin-tropomyosin-single-headed heavy meromyosin complex has been solved by three-dimensional electron microscopy using helical symmetry. Electron micrographs of negatively stained complexes were taken under minimal electron-dose conditions with higher signal-to-noise ratio than before. The resolution was 2.4 nm axially and 1.4 nm radially.

The reconstructed image recovers longer neck region of the myosin head which is almost parallel to the actin-tropomyosin filament axis, while overall structure is similar to that of actin-tropomyosin-S1. At a lower cut-off level, the neck region of the head becomes larger. S2 region cannot be reconstructed in the three-dimensional image. This means that the region near head-rod junction is mobile.

For the first time, the column-like structure that is the candidate for tropomyosin becomes continuous. The strand makes contact with the tip of the actin binding site of myosin.

The finding that the neck region is almost parallel to the filament axis strongly suggests that conformational change occurs at the bending region and/or the neck region of the myosin head during muscular contraction.

1 Introduction

Contraction of striated muscle is caused by the sliding movement between thick filaments and thin filaments (Huxley & Niedergerke, 1954; Huxley & Hanson, 1954). These two sets of filaments array themselves in an exquisitely parallel and interdigitating manner in the sarcomere, which is the structural unit of the contractile system. The thin filaments is in contact with the thick filament via cross-linkages. It is natural then to conceive the primary event leading to the relative sliding between thin and thick filaments as the interaction between these two filaments through the action of "crossbridges" (H. E. Huxley, 1969). Although there are still many important issues need to be straightened out in detail, the basic idea of "crossbridge" remains valid that it functions as an active agent capable of bridging a considerable range of side spacings between the thick and thin filaments, meanwhile transmitting the energy that is being released as a result of ATP hydrolysis in the mechanically accessible form.

It has been proven that the crossbridge originates in the thick filament which is composed largely of myosin. The head of myosin contains two functional sites, namely actin binding site and ATPase site. This fact fits in nicely with the idea of crossbridge. As the thin filament is made up mainly of globular actin monomers polymerised to double-stranded helical configuration, the actin-binding site of myosin head is that which furnishes a direct contact between thick and thin filaments. The location of ATPase site on myosin head is also consistent with the energy transduction aspect

of crossbridge.

Thus, it seems clear that, whatever the theories that postulate the probable actions of crossbridges, it is necessary to know the structure of crossbridge in detail, even to the atomic level. Since the myosin head is understood to make up the major and most important part of crossbridge, it is worthwhile to explore the possibility of knowing the structure of this part of myosin.

One approach to obtaining the structural information is through a combination of electron microscopy and image analysis. The techniques of this approach have undergone various stages of improvement and development. The structural information gathered so far has been reliable and valuable to our understanding of the molecular mechanism of contractile event.

Myosin molecule of skeletal muscle is made up of 2 heavy chains and 4 light chains. The pair of heavy chains supercoil into a rod of α-helical coiled-coil which extends from the carboxyl end to a junction called head-rod junction where the heavy chains start to fold separately into 2 heads, S1 refers to this portion of myosin, whereas S2 to that part of rod spanning the head-rod junction to a "hinge" region 60 nm from the junction. Since the first 3-D reconstruction of negatively stained actin-S1-complex (Moore *et al.*, 1970), many subsequent experimental efforts in the last 17 years have shown that the shape of the myosin head is neither cylindrical nor prolate ellipsoidal, but its overall shape looks like a pear with marked curvature. Viewed along the axis of actin-tropomyosin helix, it may look

like a banana. This pear-banana-shaped model nevertheless contains an hypothetical extrapolation from the main region of S1 to the "junction" where both heads are joined (Squire, 1983).

The electron microscopic geometry of S1 in the rigor state is established (Toyoshima & Wakabayashi, 1985a). The assignment of the domains in rigor complex has been carried out by comparing that with the electron-density map of actin-tropomyosin. The successful assignment means that the 3-D actin binding site on S1 is found. Further experimental works along the same line also reveal the 3-D locations of SH1 which is vital to the myosin ATPase. The positions of the highly positively-charged N-terminus of myosin light chain 1 and that of light chain 2 are also determined with a combination of monoclonal antibody and rotary-shadowing technique. It is found that the N-terminus of light chain 2 is located at the head-rod junction, and the N-terminus of light chain 1 is on the average 11 nm from the head-rod junction and lies in the vicinity of the actin-binding site of the myosin head. In addition, ATPase site is also located three-dimensionally. Using site-specific labelling of avidin-biotin system to the ATPase site on S1 and 3-D reconstruction of actin-tropomyosin-S1-avidin-biotin complex, it was shown that the actin binding site is 4 nm from the ATPase site which is close to the neck region. It is interesting to note that the ATPase site and actin-binding site are situated at the opposite sides of S1. With the ATPase site radially distant from the filament axis, ATP has a greater and easier access to it than if it is on the same side as actin-binding site.

Three-dimensionally reconstructed image reveals that S1 may be described as having a main region proximal to the actin-tropomyosin filament and a neck region distal to it, with a bending region in between. An important discovery from this type of structural studies is that the main region containing the actin binding site and the ATPase site does not tilt during contraction, confirming the results obtained with unlike approaches. Measurements of time-resolved changes in the low-angle X-ray diffraction pattern of contracting muscle do not register any significant variations in the equatorial pattern as predicted by the head-rotating crossbridge theory; other experiments using fluorescent probe and spin label also give negative results. These studies reveal that the probed region or the region bearing the label does not rotate during activation and contraction. And that region corresponds to the main region of S1 structurally.

Since S1 is not simply pear-shaped, an attractive possibility is that if the orientation of the main region of S1, which is almost perpendicular to the axis of the thin filament, does not change significantly throughout the ATP hydrolysis cycle, then the bending region and the neck region must be the ones that are responsible for the sliding mechanism. It has been suggested that contraction may be the outcome of the tilting in the neck region of S1, and not the main region (Toyoshima & Wakabayashi, 1985a; Tokunaga *et al.*, 1987). Accordingly, the neck region which ends at the head-rod junction is of much interest.

The objective of the present study is to obtain the structural information

of this part of the myosin, so that the structure of the whole myosin head in the rigor state may be at hand for the elucidation of the molecular mechanism of contractile event at the molecular level.

3-D reconstruction of actin-tropomyosin-S1 does not produce a clear view of the neck region because with S1 obtained by α-chymotryptic digestion, light chain 2 is lost and, as anticipated, this part of S1 is prone to fluctuation. Therefore, the density of the neck region after averaging is much lower than that of the actual. In the case of single-headed heavy meromyosin (sHMM), which we used, light chain 2 (LC2) remains although it suffers some proteolytic cleavage. We expect that the existence of this light chain will help to give better results. The usual double-headed heavy meromyosin (HMM) may do as well but it is quite clear that structural strains and asymmetry will arise in the conformation of the binding heads, since both heads do not bind to the adjacent actin monomers in the same configuration at the rigor state.

In the present study, three-dimensional structure of actin-tropomyosin-sHMM complex was solved by three-dimensional electron microscopy. The reconstructed image recovers longer neck region of the myosin head. Furthermore, the column-like structure that is the candidate for tropomyosin becomes continuous.

The finding that the neck region is almost parallel to the filament axis strongly suggest that conformational change is likely to occur at the bending region and/or the neck region of the myosin head during muscular

contraction.

2 Materials and Methods

2.1 Preparation of Proteins

Myofibrils were prepared from rabbit back muscle according to the method of Perry & Corsi (1957) with slight modifications. They were stored in 50 % glycerol (Merck) at -20 °C.

Actin was prepared from rabbit skeletal muscle acetone powder according to Spudich and Watt (1971). Tropomyosin was extracted overnight from the muscle residue with 0.6 M LiCl at pH 7.0, after troponin had been extracted with 0.4 M LiCl at pH 4.5. The crude tropomyosin was purified by the procedure described by Ebashi *et al.* (1968). Actin-tropomyosin filaments were prepared during the waiting times of the preparation of sHMM.

Single-headed HMM was prepared according to the method of K. Saeki *et al.* (personal communication). Myofibrils were washed in 4 volume of 40 mM Tris-HCl, 5 mM CyDTA and 15 mM β-mercaptoethanol at pH 8.4 twice at 25 °C for 30 minutes with gentle stirring so as to deprive about 50 % of the DTNB light chains from the myosin (Morimoto & Ohtsuki, 1986). After centrifugation at 1200 × g for 5 minutes, 4 °C , the myofibrils were washed twice with 4 volume of 10 mM Tris-HCl, 90 mM KCl and 0.1 mM DTT at pH 8.0, to get rid of CyDTA. Extraction of actomyosin and the subsequent extraction of myosin were carried out, following Cooke and Franks (1977). The supernatant which contains myosin was collected and dialysed against 10 mM imidazole and 40 mM NaCl at pH 7.0 for 3 hours in 4 °C. After sedimentation at 7,000 × g for 10 minutes, 4 °C, myosin solution

in 0.6 M NaCl, 1 mM $MgCl_2$, 1 mM $CaCl_2$ and 10 mM sodium phosphate buffer at pH 7.0 was made to a final concentration of 11 mg/ml. Starting with 25 mg of myofibrils, 16.5 mg of myosin was obtained. Proteolytic cleavage was carried out with 41.25 μl of 2 mg/ml α-chymotrypsin, 25 °C for 10 minutes. (Weeds & Pope, 1977; Okamoto & Sekine, 1985). We used 1/100 volume of 0.1 M PMSF dissolved in water-free DMF to inhibit the digestion. Dialysis was performed to equilibrate the buffer with 40 mM NaCl and 10 mM imidazole at pH 7.0 overnight, 4 °C. Separation of sHMM from HMM was done with a 16cm × 7cm column of agarose-hexane-adenosin 5′-diphosphate (AGADP, type 2 ; purchased from Pharmacia) (Mendelson & Wagner, 1984). The fraction corresponding to the peak of one-headed species was pooled (Fig. 4), dialysed against the starting buffer (10 mM NaCl, 10 mM imidazole, pH 7.0) and applied to the same column for another round of ADP-affinity chromatography. After concentration to suitable volume with Centricon centrifugal microconcentrators, separation of single-headed HMM from S1, which is another single-headed species of myosin, was performed with Superose 6 prepacked column HR 10/30 from Pharmacia. sHMM was collected as a single peak 20 to 30 minutes after injection into the HPLC system, the flow rate being 0.5 ml/min and the elution buffer was 10 mM imidazole, 0.1 M NaCl at pH 7.0 (Fig. 4). Apart from gel filtration which was done at room temperature, other procedures were carried out in 4 °C.

The fraction containing sHMM was concentrated to 0.55 mg/ml with

microconcentrator and stored on ice for later use.

SDS gel electrophoresis was done on 12.5 % poly-acrylamide slab gels using discontinuous Tris-glycine buffer system (Laemmli, 1970; O'Farrel, 1975). After fixation, gels were stained with Coomassie Brilliant Blue. Native gel electrophoresis was done on 5.5 % poly-acrylamide disk gels using discontinuous pyrophosphate-L-cysteine buffer system (Hoh *et al.*, 1976; Takano-Ohmuro *et al.*, 1983) with slight modifications. After fixation, the gels were stained with CBB.

Protein concentrations were measured by the Bradford method (Bradford, 1976), except the concentration of myosin used for the ATPase assays. Extinction coefficient E(1% at 280 nm) of myosin was taken as 5.6 $cm^{-}1$. ATPase assays were done according to the method described by Kodama *et al.* (1986).

2.2 Preparation of plastic holey film

For the purpose of negative staining and electron microscopy with minimal dose technique, it is necessary to have holes of suitable size for trapping the stain so that uniform stain sheet over the hole is formed. Plastic holey film which serves as the "mold" for the preparation of holey grids was prepared according to the protocol of Toyoshima (Dissertation thesis, University of Tokyo, 1982) with slight modifications. Microscope glass slides were cleaned with carbon tetrachloride to remove oily elements from the surface. They were left to stand in the clean vessel with a lid. All the above procedures was done in the draught. After the carbon tetrachloride had evaporated,

they were gently dipped into the distilled water. The clean slides would not have tiny water droplets adhere to the surfaces as they came out of the water. The glass were immersed into a solution of freshly prepared water repellent. Usually 0.03 % Softex KWO was used for 30 minutes. The slides were dipped again in the distilled water, to rinse gently . Any remaining droplets of water was blotted with filter paper, to make ready for the coating of plastic film.

Formation of tiny dew about 1 to 2 μm in diameter on the cooled surface of glass slide when it is transfered swiftly to room temperature and higher humility is the whole idea behind this method of preparing plastic holey film. Therefore cares should be taken to ensure that the glass surface is absolutely clean and that the room humility is not too high. By trial and error, holes with suitable size were obtainable by adjusting the time of cooling and the time allocated for dew formation, the room humility being less than 70 %. A piece of treated glass slide was cooled in the refrigerator for a suitable time, e.g. for about 60 seconds. It was then taken out of the refrigerator, and 0.3 % Triafol in ethyl acetate was poured onto the surface after about 5 seconds. The glass slide which was handled with a pair of tweezers at the shorter edge was then held over perpendicular to and the opposite side in contact with a stack of filter papers contained in the dish which lied on top of the table in the draught chamber. It took about few seconds for the excess triafol solution to be absorbed by the filter paper. Thereafter, a milky film could be observed on the glass slide.

The plastic film was examined with a phase-contrast optical microscope at the magnification of 400. Good perforated films were those for which the holes exhibited high contrast under the microscope and densely and evenly distributed over the surface, and the plastic film was not too thick that pseudo-holes were likely to be produced. A point worth mentioning is that it is quite important to absorb away the excess triafol solution at one shorter edge of the slide; the glass slide should be in contact with the stack of filter papers when triafol is drying and preferably at a constant angle, about 90 degree with respect to the surface of the table. The reason for this is that those plastic films prepared without observing this precaution, had a 99 % failure rate during the retrieval.

2.3 Preparation of holey grids

In this work, copper grids (H300 mesh from VECO) were used. The grids were first cleaned in the acetone by ultrasonic vibration. After washing and drying, a piece of filter paper on which the grids were arrayed was wetted with some mesh cement (0.2 % Neoplene rubber in toluene) in a dish so that the mesh cement wetted the grids uniformly from beneath. The grids were transferred to a fresh piece of filter paper for drying. Meanwhile, the plastic film was stripped from the glass slide by allowing to stand in the freshly made 1 % Pelex OTP solution for about 15 minutes to make it hydrophilic, and then judiciously the glass slide was dipped into a basin of still distilled water, with the slide subtending a small angle (less than 20 degree) to the surface of the water. The plastic holey film then peeled off

from the glass due to the surface tension. Grids treated with mesh cement were then transferred to lie on the plastic film which was floating on the surface of the water. Cares were taken to ensure that the side of the grid which had been treated with mesh cement was in good contact with the plastic film. A piece of light paper (backing paper of PARAFILM) larger than the plastic film was spread over the grids carefully. The paper was pressed towards the water surface so that the plastic film was glued to the grid firmly and until the paper itself was wet and the grids had adhered to the paper. The grids which were now coated with a screen of plastic film on one side were transferred to a piece of filter paper for drying. It was advisable to do this instead of leaving the grids to dry on the same piece of paper picked up from the water surface, for prolonged drying process might cause deformation of the plastic film. Good grids were selected with the aid of a phase-contrast microscope.

The next stage of preparation was carbon deposition in high vacuum (better than 1×10^{-5} Torr). A light coat of carbon was deposited followed by removal of triafol film by dissolving it in ethyl acetate. After drying, further deposition of neo-carbon was carried out. Thus, the pseudo-holes were distinguishable. Triafol plastic film was removed so as to improve thermal and mechanical stability.

The amount of carbon to be deposited, namely, the thickness of the carbon coat was decided by the average size of the hole, the population density of the hole, and above all the particular technique of negative staining and

electron microscopy. When the carbon film was excessively thick, the stain suspension trapped in the hole was substantial and vice versa. It was realized that thin carbon film tends to break under strong electron irradiation and may not allow long time of storage. However, excessively thick carbon film does not necessarily provide a strong stain film resistant to the electron irradiation, and worse, the negative staining for this is difficult and usually results in bad stain.

2.4 Preparation of Specimen for Electron Microscopy

To begin with, actin-tropomyosin filaments were prepared as follows: 6.7 μl of 6.6 mg/ml tropomyosin was mixed with 100 μl of 4.5 mg/ml actin solution. The final conditions of the solution were 0.1 M KCl, 1 mM $MgCl_2$ 10 mM Tris-HCl buffer at pH 8.0. Polymerisation of filamentous actin-tropomyosin complex was carried out in room temperature for 15 minutes.

Since the dissociation constant of sHMM to F-actin was 6.33 μM in 0.1 M KCl, 1.0 mM $MgCl_2$ 0.01 M Tris-HCl (pH 7.6) at 6 to 8 °C (Margossian & Lowey, 1973), cares were taken with regard to the concentrations and molar ratio of actin monomer and sHMM. For the purpose of 3-D reconstruction, it is indispensable to have the actin-tropomyosin-sHMM complex fully decorated and the resulting decorated filaments going straight over a distance of at least 6 cross-overs. Taking into consideration the cooperativity of the binding of sHMM to the actin-tropomyosin filaments, it was found empirically that for full decoration, the concentration of actin should be no less than 1 μM(i.e. 42 μg/ml) and the molar ratio between sHMM

and actin should be higher than 2.5.

In the present work, 2 to 3 μl of 40 μg/ml of freshly made actin-tropomyosin was mixed well with 250 μl of 0.55 mg/ml sHMM. Since rigor complex was what we required, the specimen was equilibrated through a 0.025 μm membrane filter with 1.5 mM $MgCl_2$, 0.2 mM DTT, 5 mM sodium phosphate buffer at pH 7.6, 4 °C, for more than 20 minutes and then stored on ice.

2.5 Negative staining

Negative staining was performed as follows: 5 to 8 μl of specimen was pipetted and applied homogeneously onto the carbon-coated side of the grid at room temperature. Depending on the concentration of the proteins, an interval say 5 seconds were allocated for the proteins to settle onto the carbon surface. When the concentration of the actin monomers was of the order of a few μg/ml, the grid might be overturned so that the carbon side together with the meniscus faced downward like a hanging drop. It was noted that at this posture protein filaments seemed to adhere to the carbon surface more. When the concentration of the actin monomers was as high as 40 μg/ml, this additional procedure must not be executed. Large number of filaments would be absorbed by a sufficiently hydrophilic carbon surface. Even cares should be taken to prevent over-population of filaments. The protein solution was blotted away until only a thin film was left. The specimen grid was held horizontally and 1 to 2 drops of 2 % uranyl acetate was dropped vertically onto the carbon side of the grid (Toyoshima

& Wakabayashi, 1985a). Without delay, excess stain was blotted away with a piece of torn filter paper, touching only the edge of the grid. The copper side of the grid, namely the side without carbon deposit was wiped twice gently. The specimen grid was then allowed to dry in the air for more than 15 minutes. One should not check the newly stained grids with electron microscope prematurely because it takes time for the stain trapped in the hole to stabilize itself and the stain is likely torn at the early stage by the high vacuum in the holder chamber. Thin layer of carbon about 5 nm thick was further deposited on both sides of the specimen grid according to the indirect deposition method.

All of the specimens used in the image analysis were embedded in unbroken stain sheets stretched over the holes.

2.6 Electron Microscopy

Specimen grids were examined with JEM-2000EX(JEOL) equipped with an anti-contamination device. Using the built-in minimal dose system, electron micrographs were taken, the nominal magnification being 40,000 and accelerating voltage of 100 kV. 150 μm objective aperture and 200 μm condenser aperture were used. Grids were scanned systematically at a low magnification (7,500) and low beam current (no more than 1.0 pA/cm^2 at the fluorescent screen). The electron beam was adjusted so that the would-be targets were near the fringe of the illuminated area. To increase contrast and thus making the search easier even though the illumination intensity was extremely low, the specimen was observed under underfocus conditions.

Once the target was identified, the viewing mode was switched to "focus" with the same magnification as the "photo" mode. At the "focus" mode, the beam was illuminating on the pre-set area adjacent to that which contained the targets. Here, focus, astigmatism and other necessary adjustments were done. And micrographs of the targets were taken at the photo mode where the exposure conditions were pre-set. We used 8.2 cm × 11.8 cm MEM films (Mitsubishi). Exposure conditions were chosen such that 2.8 seconds exposure time would yield an optical density of about one unit. Total electron dose was less than 10 e/Å^2. The micrographs were taken at a defocus in the range 60 to 400 nm.

The calibration of magnification was performed with the 39.5 nm periodicity in magnesium tactoids of tropomyosin (Tokunaga, personal communication; Caspar *et al.*, 1969).

2.7 Selection of good filaments for reconstruction

Micrographs were first examined by eye. Holding the micrograph obliquely, good filaments running straight over a distance of a least 6 cross-overs and apparently undistorted were selected initially. Next, they were screened by optical diffraction (Klug & DeRosier, 1966). The images that diffracted well and for which the microscope defocus was less than 400 nm, and free of other defects such as specimen drift and astigmatism were selected and printed on photographic paper. The next stage of screening was based upon the combined criteria of the quality of the layer lines, emphasizing the 6th, 1st and the 5th layer lines in that order, and the linearity of the

filament, and the homogeneity of the distribution of stain. A total of 600 micrographs were taken out of which 9 filaments were selected eventually for densitometry.

2.8 Three-dimensional Image Reconstruction

Three-dimensional image reconstruction (DeRosier & Klug, 1968; DeRosier & Moore, 1970) was performed according to Toyoshima & Wakabayashi (1985a) with slight modifications. The images selected by optical diffraction were digitized with a digital micro-densitometer MDM-6 (Joyce-Loebl) controlled with a PDP-11/44 computer (DEC). The step size of the densitometry was 20 μm. The 9 filaments were digitized and processed so that the axis of the filament was parallel to the box within an error of $\pm$ 0.15 degree as judged by the maps of auto-correlation function. Filament No. 933 was rotated virtually using the bi-linear interpolation. The rest was adjusted physically during the densitometry.

A VAX-11/780 computer (DEC) was used for image analysis. "Floating" was carried out on the edges of the box. The digitized images of the electron micrographs were Fourier transformed. Tilting of the filament out of the plane perpendicular to the electron beam was neglected, because the calculation of the tilting angle was affected by noise. Before the procedure of averaging of all the filaments, the low-resolution helical projection of each filament was calculated, using only n = 0, 2, 4, 6, 8 layer lines (The resolution was 1/9.3 nm^{-1} axially and 1/2.2 nm^{-1} radially). $\Delta\phi$, Δz and radial scale factor were roughly estimate by the helical projections, which

reduced the labour considerably in the fitting-averaging cycle. Out of the 9, a filament was chosen as the reference for the initial fitting-averaging cycle. In the course of fitting-averaging cycle, a filament with higher P_{min} was abandoned. The layer-line data up to 1/2.4 nm^{-1} (the 47th (n = 4, ℓ = 47) layer-line) in the axial direction and up to 1/1.4 nm^{-1} (the mean value) in the radial direction were used for the final Fourier-Bessel synthesis of remaining 8 filaments. Cut-off level of the three-dimensionally reconstructed image was selected so that the volume of actin-tropomyosin-sHMM become equal to the volume of actin-tropomyosin-S1 by Toyoshima & Wakabayashi (1985a).

3 Results

3.1 Preparation of single-headed heavy meromyosin

Fig.1 shows the native gel electrophoresis pattern of sHMM prepared according to the methods of Saeki *et al.* (personal communication). After extraction of about 1 of the 2 DTNB light chains from the myosin molecules, sHMM was prepared by digesting myosin with α-chymotrypsin in the presence of Ca^{2+}. Crude sHMM contained S1 and HMM (Fig. 1(a)).

ADP affinity chromatography could separate the one-headed species from the double-headed. However the peak which corresponds to sHMM and S1 contained also about 5 % of HMM. Rechromatography reduced the HMM contamination to less than 1 %. Purities were checked with gels stained by CBB. Calculations was done by integrating the areas (Fig. 1).

sHMM was finally purified from S1 by HPLC gel filtration, using Superose 6. However, we were not able to do likewise with HMM contamination. During the preliminary experiments, we were surprised to find that HMM and sHMM did not elute as separate peaks from the Asahi pack GS-620 column and Toyo Soda TSK G-4000 in series, or TSK SW4000 column either, despite the fact that the molecular weight difference between the two subfragments is as large as 100 kD.

This new preparation method largely increased the yields and shortened the preparation time. Starting with 25 mg of myofibrils, 16.0 mg of myosin was extracted and finally 0.19 mg of 99 % pure sHMM was obtained. Preparation could be performed wihtin 36 hours.

SDS-PAGE of purified sHMM shows that the heavy chain is homogeneous (Fig. 2). In the presence of divalent cations, DTNB light chains not only strengthen themselves against α-chymotrypsin but also protect the myosin head/rod junction from being cleaved. However, they are likely to undergo degradation into 17 kD fragment (Weeds & Pope, 1977). In our preparation, we obtained a stronger LC3 band, as compared to weaker LC1 band, and practically no DTNB light chain band was observable (Fig. 2). It is most probable that almost all the LC2 was degraded into 17 kD fragments, which migrated together with LC3.

In Fig. 1, we see that the two S1 isozymes are partially separated by ADP affinity column. Actually, the elution profile of the one-headed species may be considered as a superposition of sHMM, S1(A1) and S1(A2) peaks. Comparing lane (a) and (b) of Fig. 1, we find that a significant amount of S1(A1) has disappeared. Since only the early portion of the one-headed peak was collected, we could deduce that S1(A1) has stronger affinity for ADP than S1(A2).

Purified sHMM retained good ATPase activity (Fig. 5). The turn-over rates per head were summarised in Table 1. EDTA-ATPase and Ca-ATPase of sHMM were measured on the 53 hours after the start of preparation. For the control of the ATPase measurements, a portion of the myosin extracted from the CyDTA-treated myofibrils was kept on ice until the 53th hour. The sHMM which was later used for decorating actin-tropomyosin filament retained as much ATPase activity as the control myosin.

3.2 Negative staining and electron microscopy

The technique of negative staining used in this work was originated from Toyoshima & Wakabayashi (1985a) , with a slight but important modification: Specimen solution was spread on the carbon-coated side only. Compared to the Toyoshima & Wakabayashi (1985a) technique, we found that good staining results were obtained with remarkable consistency by the present method. The stain drop struck on it and got trapped in the holes; proteins were embedded in this split-second process. We found that the stain sheets produced by this method were resistant to the high illumination even before carbon backing.

During the preliminary stage of preparation of specimen grids, we used a specimen solution whose concentration was 5 times lower than the proper. It was found that the carbon-coated surface had a peculiar characteristic: more proteins would settle on to it when the meniscus was facing the ground, like a hanging drop.

Electron micrographs were taken at minimal electron-dose conditions with higher signal-to-noise ratio than previous method. The films used for this work were MEM (Mitsubishi Paper Mills Ltd.). It was found that the signal-to-noise ratio was at the saturation point when the dose was about 7 e/Å^2 with the magnification of 40,000, which gave an OD of about 1.0 (T. Matsumoto, unpublished results).

3.3 General appearance of the images

Electron micrographs of actin-tropomyosin-sHMM complex were shown in Fig. 6 and Fig. 7. They were embedded in the unbroken stain sheet stretched over the hole. Images of sHMM decorated actin-tropomyosin filaments show a characteristic arrowhead appearance. Depending on the local conditions of the stain and the orientation of binding, whiskers can be seen. They look as if they were being shot forth from the arrowheads in a wild, but not totally random manner. The most frequent place in an arrowhead where whiskers were easily spotted to be protruding was near an apex of the base of the arrowhead. Estimated roughly, the whiskers make an angle of about $\sim$ 40 degree with respect to the filament axis.

3.4 Three-dimensioanal image reconstruction

Electron micrographs used in the reconstruction was shown in Fig. 7. All the filaments were straight over a distance of at least 6 crossovers. We started off with 9 filaments which were the survivors of various rounds of elimination as described in the Materials and Methods. Since the arrowheads wear whiskers, we used a box with a larger width of 32 nm. The length of the box was tailored to accommodate exactly 6 aligned arrowheads. The selection rule of the helical symmetry was ℓ = -19n + 41m with true pitch of 110 nm.

The features of the computed transform of each filament are basically similar to the actin-tropomyosin-S1 system. Phase correlation across the meridian is good, especially for the 1 / 59 $Å^{-1}$ layer line and so called 'first'

layer line (n = 2, ℓ = 3). Phases along the layer lines vary steadily. Two of the filaments (162 and 933) give strong 1 / 27.5 $Å^{-1}$ reflection. However a strong peak which is forbidden by the selection rule also exists in the neighbourhood of the meridian at (n = 2, ℓ = 3) layer line. This reflection is not expected to be there and its origin is still obscure. It has been suggested that this reflection is the result of the uneven stain distribution (Discussion).

For refinement of the position of the helix axis, Q_{min}, the intraparticle phase residual of each filament was calculated (See Table 2). The averaged value of Q_{min} was 12.9 degree (12 pairs involved), suggesting that the departure from helical symmetry in each filament is small.

Before the average of all the filaments, the low-resolution helical projection of each filament was calculated, using only n = 0, 2, 4, 6, 8 layer lines. This image enables one to survey the individuality as well as conformity of each filament. Furthermore, approximate valued of $\Delta\phi$ and radial scaling factor could be easily estimated. Prior knowledge of these 2 parameters helps when one is about to embark on the averaging-fitting cycle. With the low-resolution helical projection, we find that filament No. 904A is most similar to the averaged appearance of all the helical projections. The other filaments do not defer that much either but look a bit queer and individualistic. We chose filament 904A as the reference and filament 872 was fitted to it. Then an average of these two filaments were produced which was taken as the reference for next round of fitting.

During the early round of fitting-averaging routine, one of the filaments was found to have larger P_{min} and was discarded. $\Delta\phi$, Δz, and scaling factor and P_{min} converge rapidly from the 4th round onwards. The average P_{min} is 49.7 degree (Table 2), suggesting that the filaments are mutually compatible.

Far sides of 8 filaments, and then near sides were separately averaged at high resolution. These 2 sets of averaged layer line data were compared. Agreements of phases at major peaks are good. Phase correlation between near and far sides of the separately averaged data was less than 80° up to 1/18 $Å^{-1}$ on many layer lines and up to 1/13 $Å^{-1}$ on several layer lines. So, the average of near side, far-side high resolution data sets were calculated. Fig. 9 displays the the averaged layer line data, which was used for the final Fourier-Bessel synthesis.

3.5 Three-dimensional image of Actin-Tropomyosin-single-headed heavy meromyosin

Fig. 10 shows the solid model of reconstructed three-dimensional image of the actin-TM-sHMM complex. The end-on view of the transparent model of helical projecion is shown in Fig. 12. Cut off level 10.5 was chosen for the solid model. This would give a volume recovery of 82 %, assuming that the specific volume was 0.74 and the molecular weight of the complex was 181K; in this estimation, the molecular weight of S2 was not included because the resulted image did not show S2 region. It can be seen that the main region binds tangentially to actin, with extensive contact. The relief

seems steeper, as one will not fail to note a necking followed by tailing of the myosin head from the front view. Whereas the axis of the main region is almost perpendicular to the filament, the neck region is almost parallel.

Another remarkable feature is that the adjacent myosin heads bound along the helix seem to have developed some form of contact with each other. Though only weakly, the main region of the myosin below is touching the neck region of the neighbour above it. We can also see the swallow-tail feature in the neck region.

Apart from these, two continuous strands of well-defined radius are seen running in the opposite "groove" of actin monomers. They also make fairly strong contact with the tip of the main region of myosin. The radius of the strand is not constant. If one imagine himself travelling up the z-axis along the strand, he will discover that the strand gets narrow immediately after it separates from the tip of the actin-myosin binding area and becoming wider as one comes nearer the next rendezvous of actin, myosin and the strand.

Comparing two helical projections, one will not fail to notice the difference between the LC2-deficient S1 decoration and LC2-subsisted sHMM decoration at high radius. sHMM decoration results in a massive and rounded appearance which is significantly different from S1. This is especially pronounced at the region 7 nm from the axis. Whereas the density in this region of S1 is low, from the untwisted projection map of sHMM, it is evident that in the corresponding region, the density distribution has a

well-defined peak.

At this cut-off level, nothing is visible beyond the neck region of myosin. But when the cut-off level is set at 5.5, we can see some novel features at higher radius. A piece of low-density mass appears to stick out from the neck region tangentially. It is remarkable that even with this low cut-off level, our reconstruction data are not noisy at the high radius-periphery, unlike the S1's, which have a lot of disconnected arc-like streaks of considerable density floating at high-radius.

4 Discussion

4.1 Preparation of single-headed heavy meromyosin

Preparation of sHMM by the method of Saeki *et al.*(1988) results in pure and homogeneous one-headed specimen. Unlike α-chymotryptic S1, for which all the LC2's are lost, our sHMM still retains LC2, though suffer some cleavage. It is likely that the surviving 17-kD fragment of LC2 still associates with the heavy chain.

Our prescription of cleaving CyDTA-treated myosin is exactly the copy of the original formula by Weeds & Pope (1977). It is curious that with 0.05 mg / ml of α-chymotrypsin for 10 min at high ionic conditions and 25 °C in the presence of divalent ions, most of the LC2's are intact for normal myosin (Weeds & Pope, 1977); but in the case of CyDTA-treated myosin, most of the LC2's degrade into 17 kD fragment. Thus it seems that when one of the myosin heads is deprived of LC2, the remaining LC2 on the other head is more susceptible to proteolytic cleavage to smaller fragment. This result is comprehensible because the molar ratio of α-chymotrypsin to LC2 in our preparation was about two times higher than that in the preparation of HMM by Weeds & Pope's method. It would be better if the digestion conditions for the CyDTA-treated myosin were 50 % milder. Perhaps it is beneficial if the digestion is done at 4 °C.

Although the role of LC2 is still putative, it is nevertheless very important to have the LC2 as intact as possible for the 3-D reconstruction. This is because various studies have indicated that the mobility in the head/rod

junction is attenuated upon binding of actin to the main part. This mode of interaction is highly LC2 dependent. It has been found that the integrity of LC2 has profound effects on the binding of myosin head to actin. Miller & Reisler (1985) discovered that when LC2 is degraded to 17 kD, it can no longer assume the function of signal transduction between the main part of the head and the head/rod junction. Since the N-terminal amino acid residues of LC2, which are localized at the head/rod junction, are the ones digested by the proteinases, we can not expect the remaining 17 kD-fragment to do as good as the intact LC2 in strengthening the head/rod junction. The inability of present study to see S2 may have its indirect cause in this.

When LC2 is intact, the chymotryptic cleavage of head/rod junction will be inhibited by actin binding (Miller & Reisler, 1985). An improvement of the Saeki *et al.* method may be that the digestion should be done with partially LC2-deficient actomyosin, namely, before extraction of partially LC2-deficient myosin from actomyosin.

4.2 Quality of the data

The quality of our data is high, despite the fact that we are reconstucting with sHMM which is larger than S1. At first, we expected that the signal-to-noise ratio of the micrographs of actin-tropomyosin-sHMM would be inferior to that of the actin-tropomyosin-S1. In many ways, sHMM is less stable than S1. S2 moieties might even interfere with the formation of arrowheads. However, the final results of our reconstruction show that this

is not true. For the first time, we are able to show clearly two *continuous* strands lying on the opposite outskirts of actin filament. This is one of the evidence testifying that the quality of the present data is very high.

Puzzling as it may seem, we can name three factors contributing to the improvement of signal-to-noise ratio and resolution over previous works. First, the photographic films we used to record images in this work were MEM. In the previous works, Kodak 4463 or AA were used . Given that the films were developed with optimum conditions, it could be that MEM is superior to 4463 or AA in signal-to-noise ratio. This factor could be gauged quantitatively by comparing the dose response curves and the modulation transfer functions of the respective films. Secondly, as has been described in detail in the Materials and Methods, the staining technique is slightly different. Instead of applying specimen solution on both sides of the grid, we applied the solution to the carbon-coated side *only*. The rest of the staining procedures were basically the same as previous. It could be that without the specimen solution applied on the copper side, preservation of protein structures is more advantageous and fidel than if some solution was there, which might affect the overall distribution of stain in an adverse manner. Indeed, the stain distribution cuves of the two samples were slightly different (Fig. 13). Thirdly, contrary to the early belief, it could also be that sHMM is inherently more suitable for decoration than the LC2-deficient S1. The head/rod junction may has profund infuences over the way main part of myosin binds to actin, so that in return the stability of the junction

is enhanced. Lastly, the amount of dose used for recording is different. Toyoshima & Wakabayashi (1985a) used only 5 e / Å ^{2}. We used 8 e / Å ^{2}. It is reasonable to assume that the difference in radiation damage between the two doses is small, whereas the signal-to-noise ratio is higher for higher dose.

4.3 Overall structure of the myosin head

One of the conclusions from the 3-D reconstruction of rigor complex of actin-tropomyosin-sHMM is that this system reproduces essentially the same kind of geometry of the main region of myosin head as those derived from other rigor complexes. The results also agree remarkably with the 3-D maps from cryo-electron microscopic images of S1-decorated thin filaments frozen in thin aqueous films (Milligan & Flicker, 1987). All these similarities point to the fact that the main region of S1 is highly rigid, at least in the rigor state. This is not surprising. From the point of view of free energy and thermodynamic stability, it is more profitable for the myosin head to associate with F-actin in the absence of ATP. Fig. 12(d) is obtained with a cut-off level 14.8. It can be seen that the overall shape of the main region of myosin head is also independent of the contour levels in the range 10 to 15. The structural information of this portion is most reliable of all.

There is some subtle difference in the density distribution of the main part between our map and the one by Toyoshima & Wakabayashi (1985a) (Fig. 12).

Our model agrees well with the results of negatively stained actin-tropomyosin-S1 and the results of S1-decorated thin filaments by cryo-electron microscopy. We like to iterate that S1 binds to one actin monomer in the filament. The interaction between S1 and actin is strong and spatially extended, as the contact area is large.

We can also notice a striking resemblance between our myosin head seen in the helical projection with the section of crystalized S1 (Winkelmann *et al.*, 1985).

4.4 Structure of the neck region of the myosin head

With the cut-off level at 10.5 (82 % volume recovery), the reconstructed image recovers longer neck region of the myosin head. The neck region is almost parallel to the actin-tropomyosin filament axis (Fig. 10 & Fig. 11).

Our helical projection map is also roughly similar to that derived from the scallop myosin S1 which retains the regulatory light chain (Vibert & Craig, 1982). The rounded appearance at a distance 7 nm from the centre is contrasted with the low-density profile of α-chymotryptic S1 (Fig. 12). It is justified to conclude that the increased massiveness in this part is due to the presence of LC2. This conclusion is supported by two facts. Firstly, sHMM differs from S1 by having LC2 and S2. Secondly, LC2 is known to associate with the span of neck region of myosin head, whereas S2 probably does not. Since our results and that of the scallop S1 are qualitatively similar at this distance from the centre, it can be inferred that the increased massiveness is the result of the presence of S2. However,

we are not sure if the increased mass is LC2 itself, or the neck region of heavy chain rendered visible indirectly by the stabilizing effects of LC2, or a combination of both.

4.5 Structure of S2 and head-rod junction

When the cut-off level is 5.5 (about 120 % volume recovery), we do not see further tailing parallel to the filament axis. Instead, the whole complex swells rather isotropically. It is noteworthy that the tip of the neck region which was pointed at 10.5 cut-off level acquires a new feature. A piece of mass seems to stick out from the end of the neck region in the clockwise direction as indicated by arrows in Fig. 11 and Fig. 12. Without extra information, it is hard to assign a meaning to it. Nevertheless, this feature is not an artefact because it is an connected extension of the neck region. We shall call it as collarette.

If one is allowed to be less punctilious, one will exclaim that this could well be the beginning of head-rod junction. Indeed, Katayama & Wakabayashi (1981) report that a *filamentous* domain appear to wind clockwise around the main body of the structure when viewd from Z-line. They strongly hint that it may correspond to a relatively rigid part of S2. Our helical projection contoured at 5.5 cut-off level is essentially similar to theirs. It is likely that their filamentous domain is our collarette. But we want to contend that at least our collarette is not S2. S2 is filamentous and far away from the axis of the rigor complex. It is joined to the myosin head at the head/rod junction. Knight & Trinick (1984) report that the head is

free to swing about its junction with the neck region. From time-resolved optical anisotropy decay measurements, Kinoshita *et al.*(1984) found that the wobbling motion of the head can be understood better by postulating yet another swivel located in that part of S2 closer to the head. It can be said that in the neighbourhood of head/rod junction, the polypeptides are very flexible. Therefore, it is improbable for S2 not to depart from the helical symmetry. Correspondingly, S2 is interdicted from being unveiled by the present reconstruction method, which makes no provision for the treatments of non-helical configuration. Despite seeing whiskers coming out from the filament main body (Fig. 6), it is quite impossible to pick them up from the noisy ambience by the present method of image analysis.

S1 comprises the major portion of myoisn head; it has been argued that there is still some distance from the end of the neck region of S1 to the head/rod junction (Squire, 1981). Three possibilities, therefore, are conceivable with the novel protrusion: It may be that this low-density mass is still a part of S1. Or, it is possible that the novel feature is not a part of S1 but it may well be the starting point of the hypothetical stretch spanning the end of S1 neck region to the head/rod junction. Or it could be the head/rod junction itself. Granted that the novel feature is not artificial, we shall discuss that it is not the head/rod junction.

Although it is still controversial, reliable estimations from various approaches agree that that the length of myosin head should be greater than 17 nm and less than 21 nm when heads are detached from actin. As the

geometry of myosin head is not simple, we note that the estimations are very interpretation-dependent. Nevertheless, we attempt to give 15.5 nm as the longest chord for our model contoured with 100 % volume recovery. Thus we see that the collarette can not be the head/rod junction itself.

When thin sections cut parallel to the [100] plane from the negatively stained papain-S1 crystals were examined by electron microscopy, the length of the molecule was 16 nm (Winklemann *et al*, 1985). Since the estimation for our model is compatible to their results, we would conclude that the collarette may be still S1. If this is true, then we realize immediately that even the shape of the neck region is not as simple as we had imagined. There may be yet another bending region in the neck region of S1.

On the other hand, the collarette is the outcome of contouring our map with a volume recovery greater than 100 %. This mean that the collarette does not belong to the 181-kD rigor complex. Although the *de facto* molecular weight of actin-tropomyosin-sHMM should be about 235 kD, our volume recovery was calculated with 181 kD, 20 kD heavier than the LC2-deficient actin-tropomyosin-S1. This is reasonable because the 57 kD-S2 is not visible in our reconstruction. We suppose that 181 kD is a good figure for a LC2-intact actin-tropomyosin-S1 complex. So, if we argue by volume recovery, which is dependent on the assumption of molecular weight, we could conclude that the collarette does not belong to S1, but the remaining myosin head.

Whether the collarette is a part of S1 or not remains curious.

4.6 Structure of actin

Our helical projection map shows that the density distribution of actin is somewhat different from that of Toyoshima & Wakabayashi (1985a). Two well-defined regions of high density can be recognized. One region is larger than the other. Myosin head binds to the larger one. For comparison, we note that in the helical projection map of actin-tropomyosin-S1, there are 3 high-density regions in each actin monomer. Two of them are about the same size, the remaining one (domain A1) is a bit larger and S1 is binding to it.

4.7 Structure of tropomyosin

A continuous strand of column-like structure is clearly seen in our model (Fig. 10). This is very reminiscent of the 3-D reconstruction of actin-tropomyosin paracrystals by O'Brien *et al* (1983). Though not confirmative, we strongly suggest that it is tropomyosin.

The continuous strand is about 4 to 4.5 nm from the axis. The diameter of the strand is not constant; it is largest at the lower end of the rendezvous with actin and myosin, and smallest at the upper end from where the strand is out of contact with the main body until the next rendezvous. This picture is consistent with the findings of Phillips Jr *et al* (1986).

4.8 Molecular mechanism of muscular contraction

That the head of myosin alone and not the S2 or rod moiety is sufficient for the contractile event in the actin-myosin motility system such as muscle,

is not at all trivial. A series of ingenious movement assays concluded that the power stroke needs only the S1 and nothing more (Toyoshima *et al.*, 1987), thus dismisses convincingly the hypothesis that the power stroke is generated by the helix-random coil transition at the "hinge" region of S2.

The tilting mechanism (H.E. Huxley, 1969) of myosin head has been a working hypothesis for the molecular mechanism of muscle contraction. In this mechanism, tilting of the whole head has been usually assumed. However, many experiments have proved otherwise. For example, fluorescent or spin-labelled ATP or ADP bound to myosin did not change its angle to the axis of the actin filament during muscular contraction (Yanagida, 1981; Crowder *et al.*, 1985).

It was suggested, thereafter, that muscle contracts by tilting the neck region of S1, not the main region (Toyoshima & Wakabayashi, 1985a; Tokunaga *et al.*, 1987). This work shows that the angle between the main region and the neck region of the myosin head is about 90 degree in the rigor state. It is still premature to assign a meaning to this finding, although it is quite alright to say that either the bending region becomes rigid at the end of the power stroke, (If the bending region were still mobile, we would not have seen the tailing neck region.) or it is inherently rigid in the accompaniment of LC2.

One must not presuppose that flexibility of certain regions is *the* necessary and sufficient proof of tilting mechanism. If a certain region is flexible throughout the ATP cycle, it is impossible for it to play the role of transmit-

ting the force. Physics teaches that rigidity is required if the lever system is to work properly. Therefore the rigidity of the bending region in the rigor state, which is thought to be the end of the power stroke, and the finding that the neck region is almost parallel to the axis of the filament suggest strongly that conformational changes at these regions is responsible for the sliding.

Acknowledgement

I thank Professor Takeyuki Wakabayashi for suggesting this work, many helpful advices and reading the manuscript. I am grateful to Miss Kimiko Saeki and Dr Makio Tokunaga for collaboration in this study. I am greatly indebted to Dr C. Toyoshima, Dr A. Tomioka and Mr T. Matsumoto for the use of programs written by them. I thank Professors T. Yamazaki, T. Kamae and the system managers of VAX-11/780 for making VAX-11/780 available to us and Dr L.A. Amos, who kindly provided a program package for processing large image arrays.

References

Amos, L.A., Huxley, H.E., Holmes, K.C., Goody, R.S. & Taylor,K.A. (1982). Nature, **299**, 467-469.

Bradford, M.M. (1976). Anal. Biochem. **72**, 248-254.

Caspar, D.L.D., Cohen, C. & Longley, W. (1969). J. Mol. Biol. **41**, 87-107.

Cohen, C. (1980). J. Mol. Biol. **140**, 35-55.

Cooke, R., Franks, K. E. (1977). J. Mol. Biol. **120**, 361-373.

DeRosier, D.J. & Klug, A. (1968). Nature, **217**, 130-134.

DeRosier, D.J. & Moore, P.B. (1970). J. Mol. Biol. **52**, 355-369.

Ebashi, S., Kodama, A. & Ebashi, F. (1968). J. Biochem. **64**, 465-477.

Eisenberg, E. & Hill, T.L. (1985). Science, **227**, 999-1006.

Elliott, A. & Offer, G. (1978). J. Mol. Biol. **123**, 505-519.

Flicker, P.F., Wallimann, T. & Vibert, P. (1983). J. Mol. Biol. **169**, 723-741.

Hibberd, M.G. & Trentham, D.R. (1986). Ann. Rev. Biophys. Biophys. Chem. **15**, 119-161.

Hoh, J.F.Y., MacGrath, R.I. & White, R.I. (1976). Biochem. J., **157**, 87.

Huxley, A.F. & Niedergerke, R. (1954). Nature, **173**, 971-973.

Huxley, H.E. (1969). Science, **164**, 1356-1366.

Huxley, H.E. & Hanson, J. (1954). Nature, **173**, 973-976.

Katayama, E. & Wakabayashi, T. (1981). J. Biochem. **90**, 703-714.

Klug, A. & DeRosier, D.J. (1966). Nature, **212**, 29-32.

Kodama, T., Fukui, K. & Kometani, K. (1986). J. Biochem. **99**, 1465-1472.

Laemmli, U.K. (1970). Nature, **227**, 680-685.

Lowey, S., Slayter, H. S., Weeds, A. G. & Baker, H. (1969). J. Mol. Biol. **42**, 1-29.

Margossian, S.S. & Lowey, S. (1973). J. Mol. Biol. **74**, 313-330.

Mendelson, R.A. & Wagner, P.D. (1984). J. Mol. Biol. **177**, 153-171.

Miller, L. & Reisler, E. (1985). J. Mol. Biol. **182**, 271-279.

Milligan, R.A. & Flicker, P.F. (1987). J. Cell. Biol. **105**, 29-39.

Moore, P.B., Huxley, H.E. & DeRosier, D.J. (1970). J. Mol. Biol. **50**, 279-295.

Morimoto, S. & Ohtsuki, I. (1986). J. Biochem. **101**, 291-301.

O'Brien, E.J., Couch, J., Johnson, G.R.P. & Morris, E.P. (1983) Actin Structure and Function in Muscle and Non-Muscle Cells, dos Remedios, C.G. & Barden, J.A., Eds, Academic Press, Sydney.

Okamoto, Y. & Sekine, T. (1985). J. Biochem. **98**, 1143-1145.

O'Farrell, P.H. (1975) J. Biol. Chem. **250**, 4007-4021.

Perry, S.V. & Corsi, A. (1957). Biochem. J. **68**, 5-12.

Phillips Jr, G.N., Fillers, J.P. & Cohen, C. (1986). J. Mol. Biol. **192**, 111-131.

Spudich, J.A. & Watt, S. (1971). J. Biol. Chem. **246**, 4866-4871.

Squire, J. (1981). The Structural Basis of Muscular Contraction, Plenum Press, New York.

Takano-Ohmuro, H., Obinata, T., Mikawa, T. & Masaki, T. (1983). J. Biochem. **93**, 903.

Taylor, K.A. & Amos, L.A. (1981). J. Mol. Biol. **147**, 297-324.

Tokunaga, M., Suzuki, M. Saeki, K. & Wakabayashi, T. (1987). J.Mol.Biol. **194**, 245-255.

Tomioka, A., Tokunaga, M. & Wakabayashi, T. (1987). submitted to J.Mol.Biol.

Toyoshima, C. & Wakabayashi, T. (1985a). J. Biochem. **97**, 219-243.

Toyoshima, C. & Wakabayashi, T. (1985b). J. Biochem. **97**, 245-263.

Toyoshima, Y.Y., Kron, S.J., McNally, E.M., Niebling, K.R., Toyoshima, C., & Spudich, J.A. (1987). Nature **328**, 536-538.

Vibert, P.& Craig, R. (1982). J. Mol. Biol. **157**, 299-319.

Wagner, P.D. & Weeds, A.G. (1977). J. Mol. Biol. **109**, 455-473.

Wakabayashi, T. & Toyoshima, C. (1981). J.Biochem. **90**, 683-701.

Wakabayashi, T., Huxley, H.E., Amos, L.A. & Klug, A. (1975). **93**, 477-497.

Weeds, A.G. & Pope, B. (1977). J. Mol. Biol., **111**, 129-157.

Weeds, A.G. & Taylor, R.S. (1975). Nature, **257**, 54-56.

Winkelmann, D.A. & Lowey, S. (1986). J. Mol. Biol. **188**, 595-612.

Winkelmann, D.A., Mekeel, H., & Rayment, I. (1985). J. Mol. Biol.**181**, 487-501.

Yanagida, T. (1981). J. Mol. Biol. **146**, 539-560.

Figures & Tables

Table 1

Enzymic activities of sHMM and control myosin

	μmole Pi / mg enzyme / min		turn-over rate per head (sec^{-1})	
	Ca^{2+}-ATPase	EDTA-ATPase	Ca^{2+}-ATPase	EDTA-ATPase
Myosin	0.12	0.30	0.49	1.2
SHMM	0.13	0.28	0.49	1.0

Table 2

Intraparticle and interparticle phase residuals of the 8 particles used in 3-D reconstruction

Image	Intraparticle phase residuals		Interparticle phase residuals	Radial scaling factor
	Q_{min} (degree)	Number of peaks incorporated[a]	P^b (degree)	
904A	13.8	14	41.8	1.01
872	11.2	12	49.0	0.95
893	14.7	12	50.2	0.92
162	14.3	14	47.1	0.94
933	8.8	11	50.4	0.85
904B	13.4	9	56.6	0.97
935	10.8	14	49.0	0.95
146	16.3	10	53.7	0.91
Average	12.9	12	49.7	0.94

a. Number of peaks involved in the calculation of Q_{min}(defined by DeRosier & Moore, 1970).

b. Calculated at the resolution of 1/ 2.2 nm^{-1}, using the 6, 9, 10, 13, 16, 19, 22, 25 and 41th layerlines (P; defined by Wakabayashi *et al* ., 1975).

Fig. 1. Native gels of **(a)** crude sHMM, **(b)** after ADP-affinity chromatography, and **(c)** after ADP-affinity rechromatography. The gels show that HMM contamination is less than 1 %. The S1 contamination is removed by gel filtration (Fig. 2 & Fig. 4).

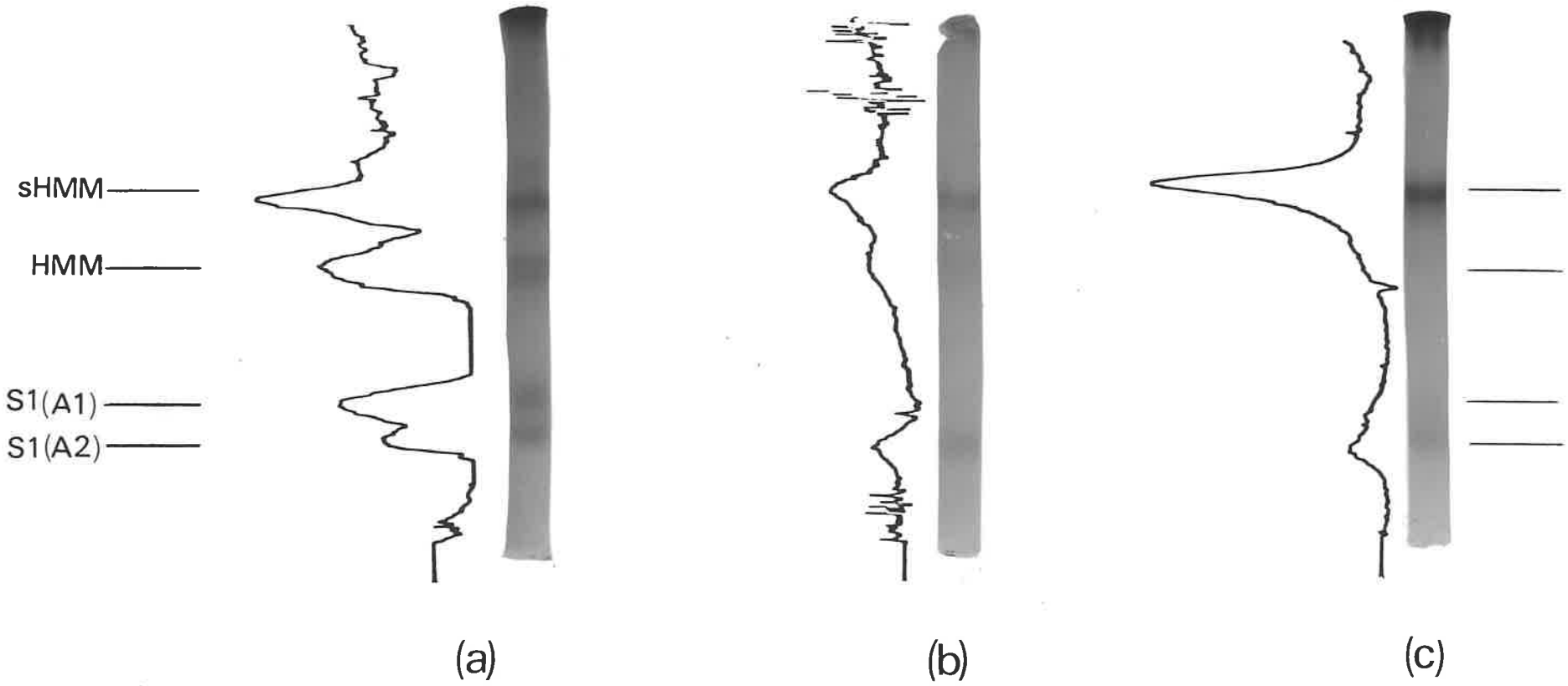

Fig.1.

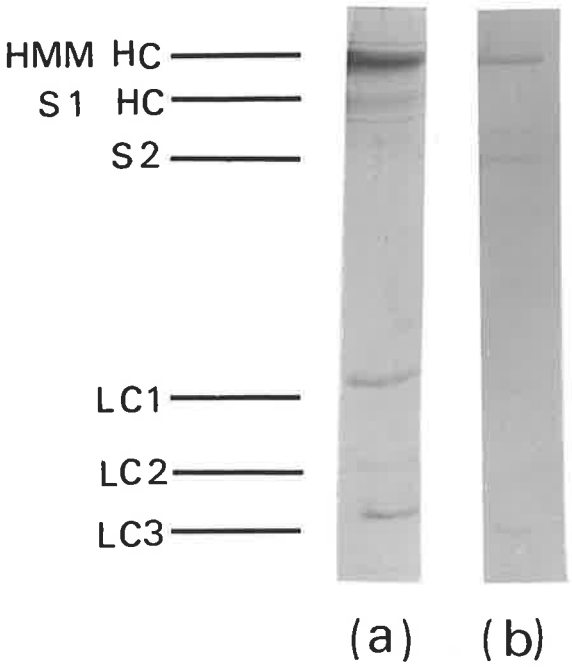

Fig. 2. SDS-acrylamide gel electrophoresis (12.5 % gel) of (a) a mixture of HMM and S1 as marker, and (b) sHMM after gel filtration. Gels were stained with CBB.

Fig. 3. ADP-column elution profile of **(a)** first chromatography and **(b)** rechromatography. The first arrow indicates a step to 75 mM NaCl. The second arrow indicates a step to 1 M NaCl in the salt concentration of the elution buffer. The shaded area indicates the fraction collected. The flow rate was 18 ml/hr. Absorbance was measured at 280 nm. Separation of one-headed species from two-headed on AGADP affinity chromatography column was done in 8 °C. In fig.3(a), 1.2 ml of about 6 mg/ml solution of crude products from α-chymotryptic digestion was applied to a 16 cm × 0.7 cm colum of agarose-hexane-adenosin 5'-diphosphate (AGADP, type 2 from Pharmacia). Starting buffer was 10 mM NaCl. Single-headed species namely sHMM and S1 were eluted by a step to 75 mM NaCl. HMM was eluted by a step to 1 M NaCl. In fig. 3(b), after the fraction collected from first chromatography was dialysed against the starting buffer for 2 hours, 7.4 ml of about 0.25 mg/ml protein solution was applied for rechromatography.

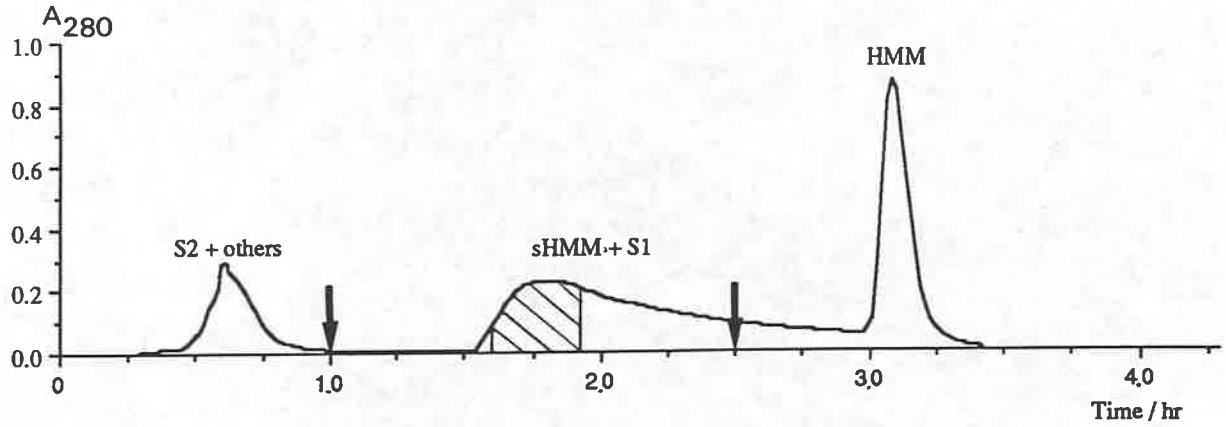
A280
1.0
0.8
0.6
0.4
0.2
0.0
S2 + others
sHMM + S1
HMM
0
1.0
2.0
3.0
4.0
Time / hr

fig. 3(a).

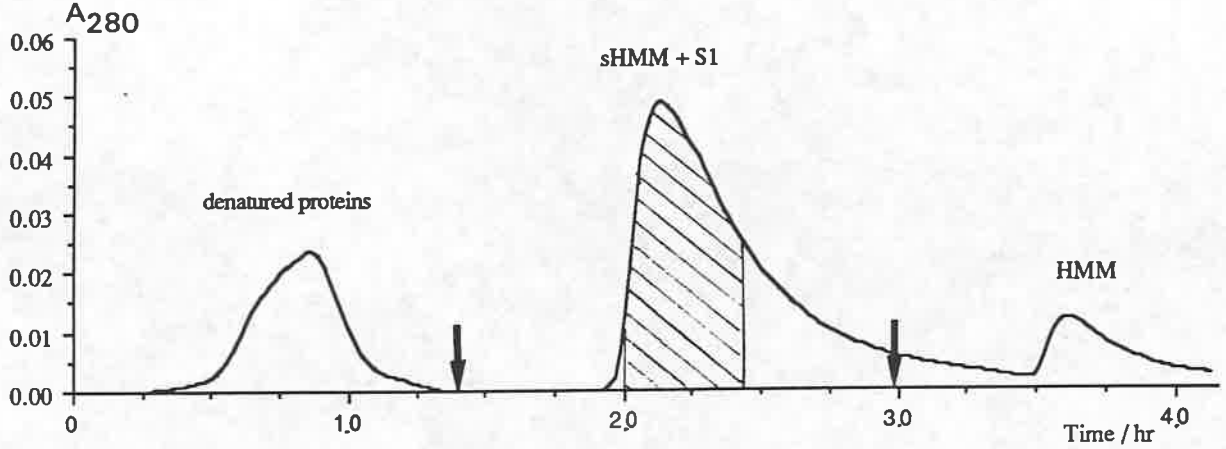
A280
0.06
0.05
0.04
0.03
0.02
0.01
0.00
sHMM + S1
denatured proteins
HMM
0
1.0
2.0
3.0
4.0
Time / hr

fig. 3(b).

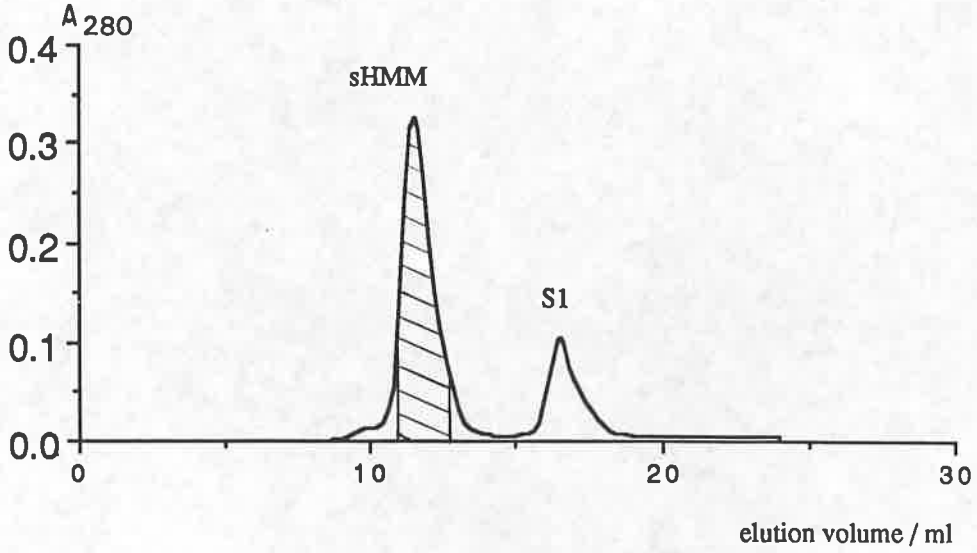

Fig. 4. Gel-filtration profile of the fraction after ADP-affinity rechormatography. The shaded area indicates the fraction collected. sHMM was separated from S1 on Superose 6 by HPLC was done. About 1 ml of 0.3 mg protein solution was applied to a 30 cm x 1 cm column and eluted with a buffer containing 10 mM imidazole and 0.1 M NaCl (pH 7.0). The flow rate was 0.5 ml/ min. Absorbance was measured at 280 nm.

Fig. 5. ATP assays were carried out at 25 °C and pH 7.0. For the Ca-activated ATPase, the final mixture contained 0.5 M KCl, 10 mM imidazole-HCl, 2 mM ATP and 10 mM $CaCl_2$. For the EDTA-activated ATPaes, the conditions were the same except $CaCl_2$ was replaced by 2 mM EDTA. 21.7 μg of myosin or 9.5 μg of sHMM in a total volume of 1 ml were used. Inorganic phosphate released was measured by the method described by Kodama *et al.* (1986).

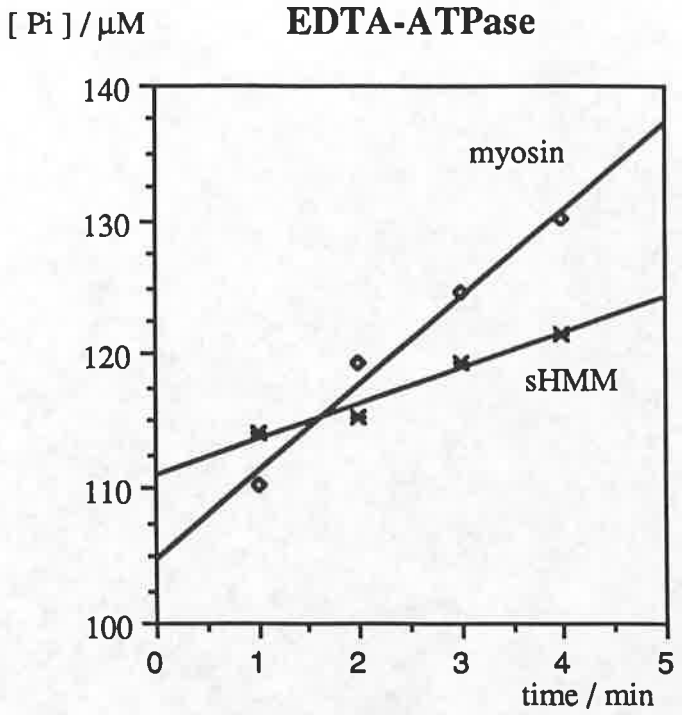
[Pi] / μM
EDTA-ATPase
140
130
120
110
100
0
1
2
3
4
5
time / min
myosin
sHMM

fig. 5(a).

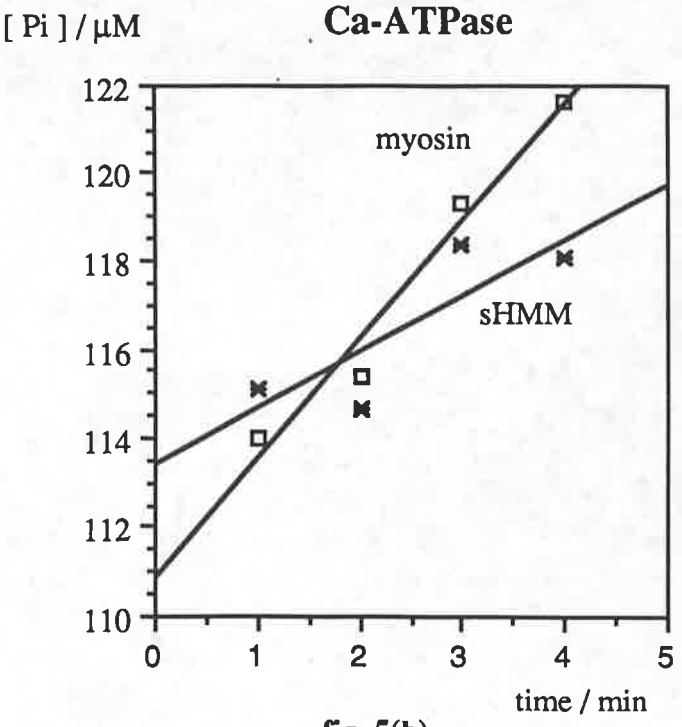
[Pi] / μM
Ca-ATPase
122
120
118
116
114
112
110
0
1
2
3
4
5
time / min
myosin
sHMM

fig. 5(b).

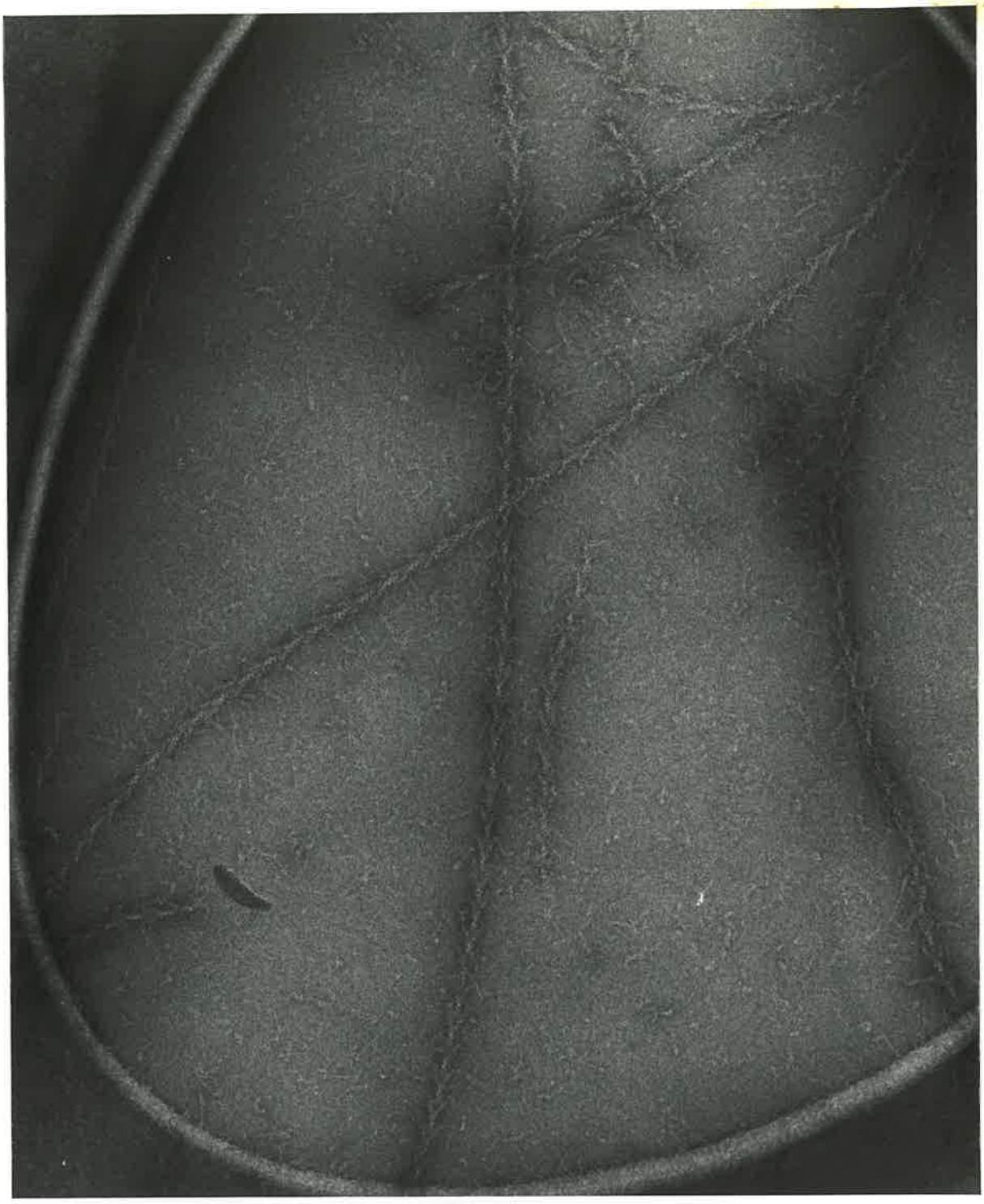

Fig. 6. Field of an electron micrograph of the actin-tropomyosin(TM)-sHMM complex. The specimen was negatively stained with 2 % uranyl acetate and embedded in unbroken stain films suspended over holes (Proteins look white). Electron micrographs were recorded by minimal electron-dose technique. Notice that S2 is visible. Bar represents 100 nm.

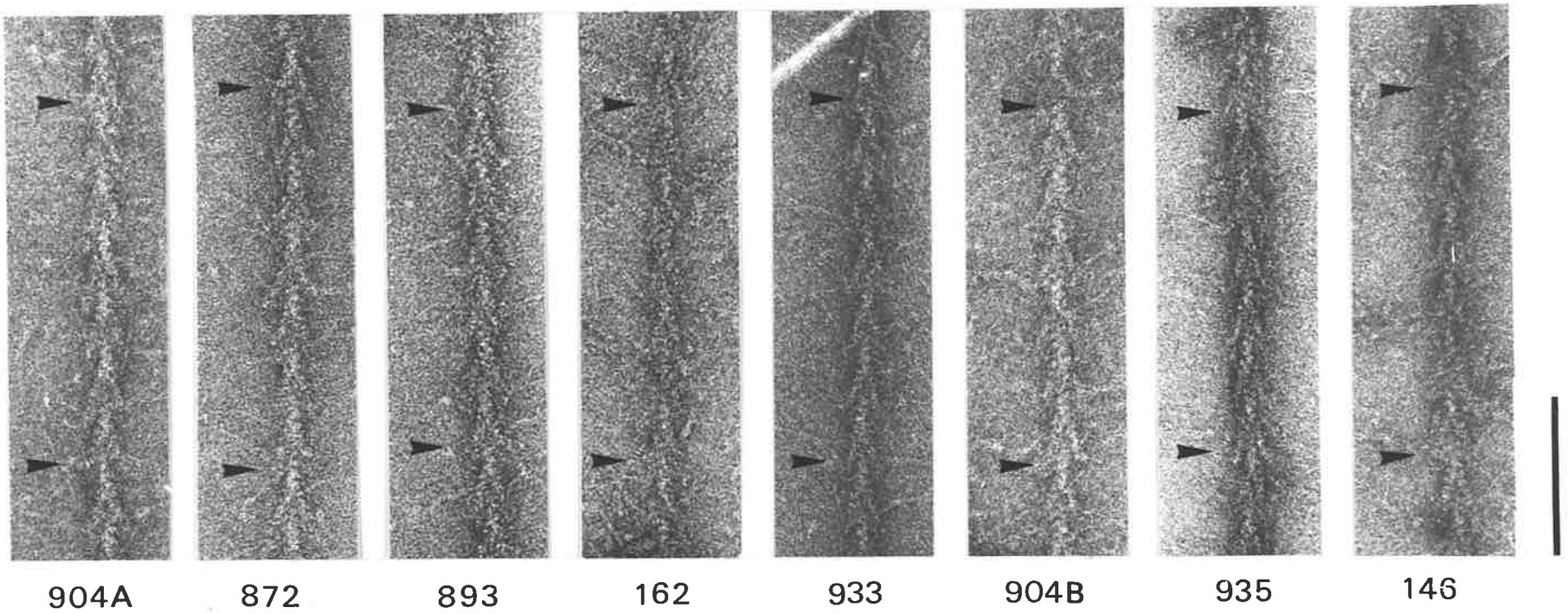

Fig. 7. Gallery of the electron micrographs of the actin-TM-sHMM complex. The region whose both ends were pointed by arrowheads were used in the three-dimensional image reconstruction. The actin-TM filament was decorated with sHMM in the absence of ATP. Note that arrowhead appearance is distinct and a part of S2 is visible at the base of the triangle arrowhead. Bar represents 100 nm.

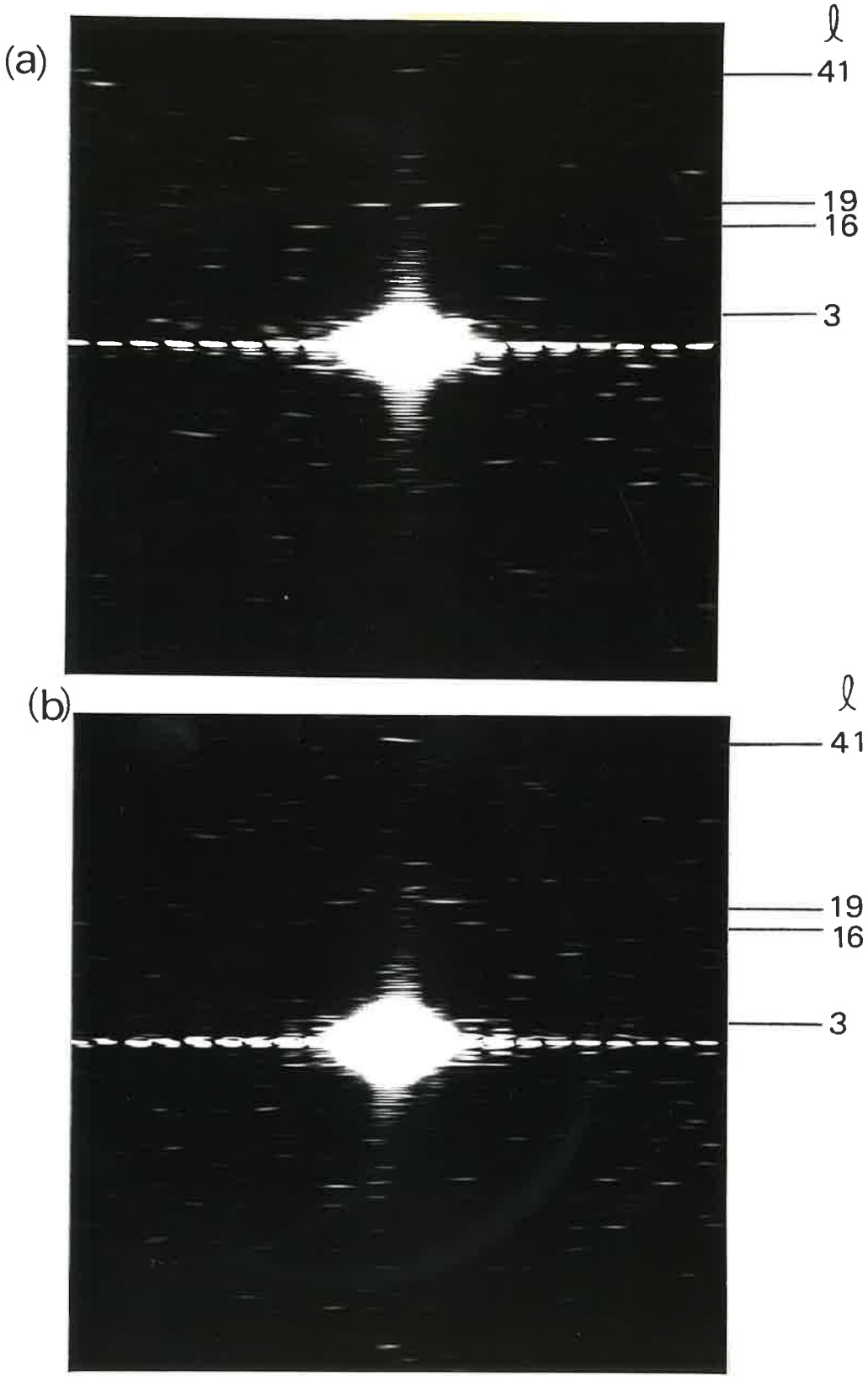

Fig. 8. Typical optical diffraction patterns of the electron micrographs of actin-TM-sHMM shown in Fig. 7 ((**a**), identification number 904A; (**b**), identification number 162.)

Fig. 9. Amplitude distributions along the layer-lines after averaging data from 8 images of the actin-TM-sHMM complex shown in Fig. 7. Abscissa indicates radius in the Fourier space. The orders of Bessel function (n) and the layer-line numbers (l) are shown in parentheses as (n,l).

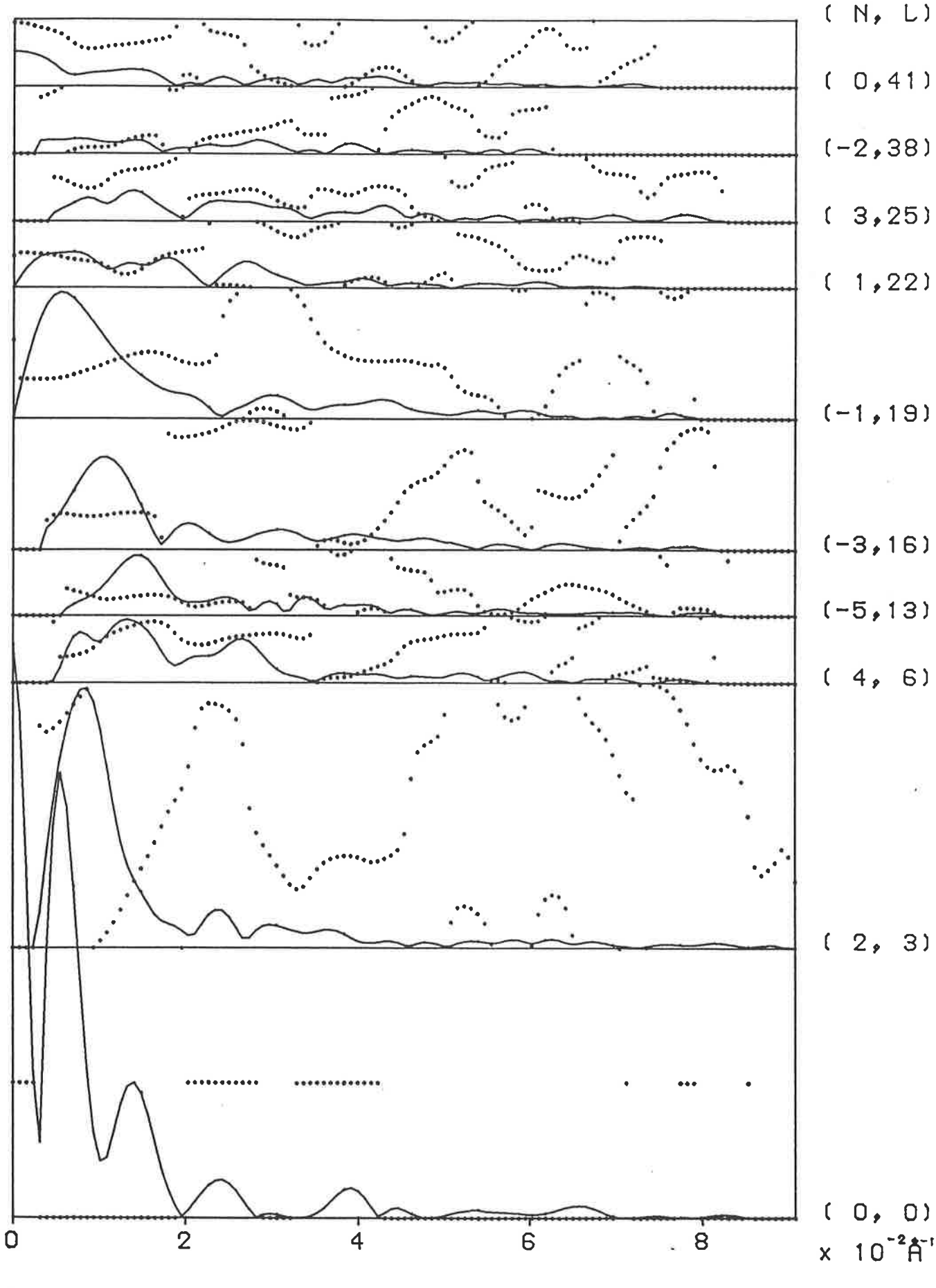

Fig.9.

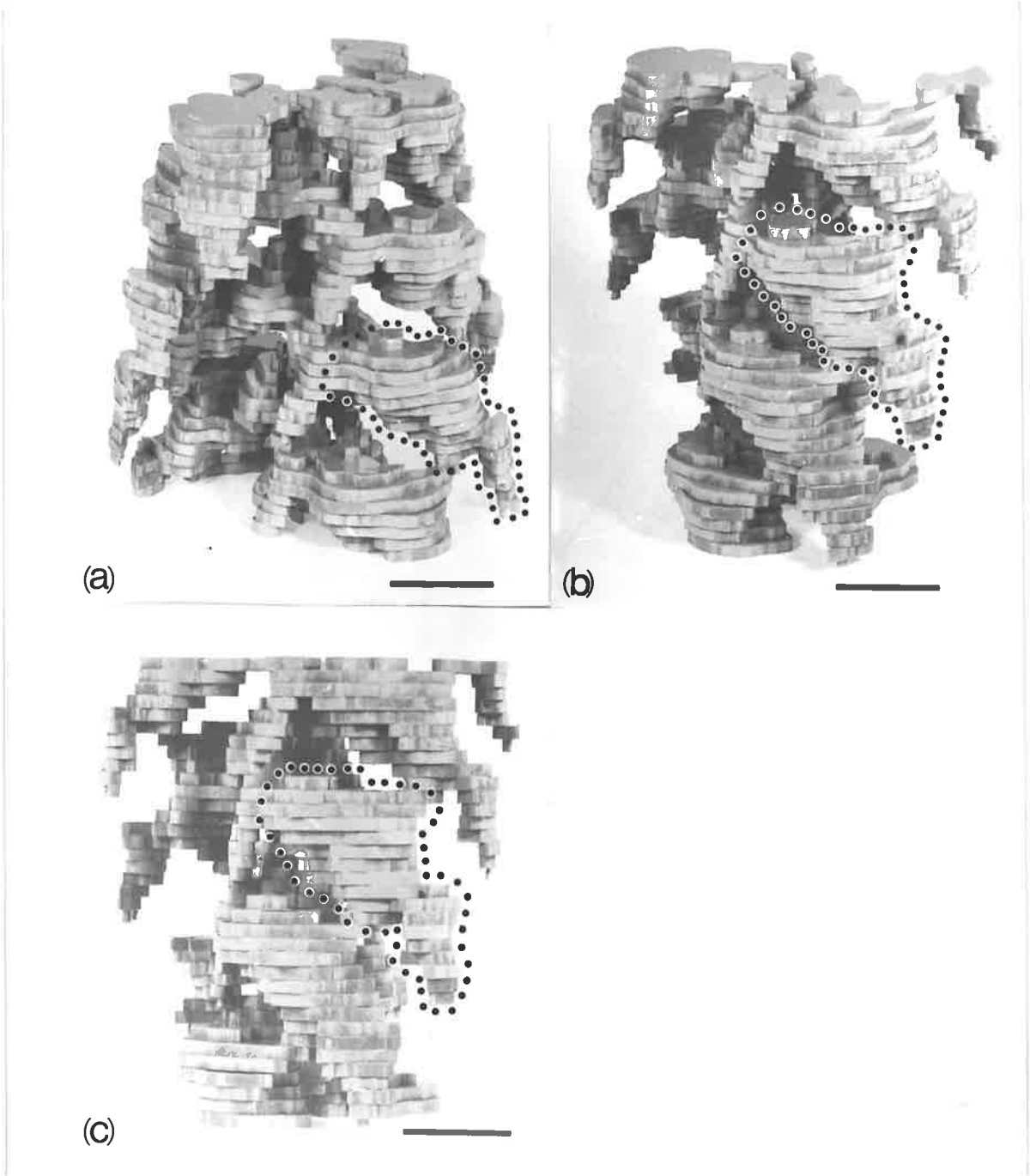

Fig. 10. The solid model of the reconstructed image of actin-TM-sHMM. The three-dimensional image was reconstructed from the electron micrographs shown in Fig. 7, using the helical symmetry. The volume recovery is 82 %. Bar represents 5 nm.

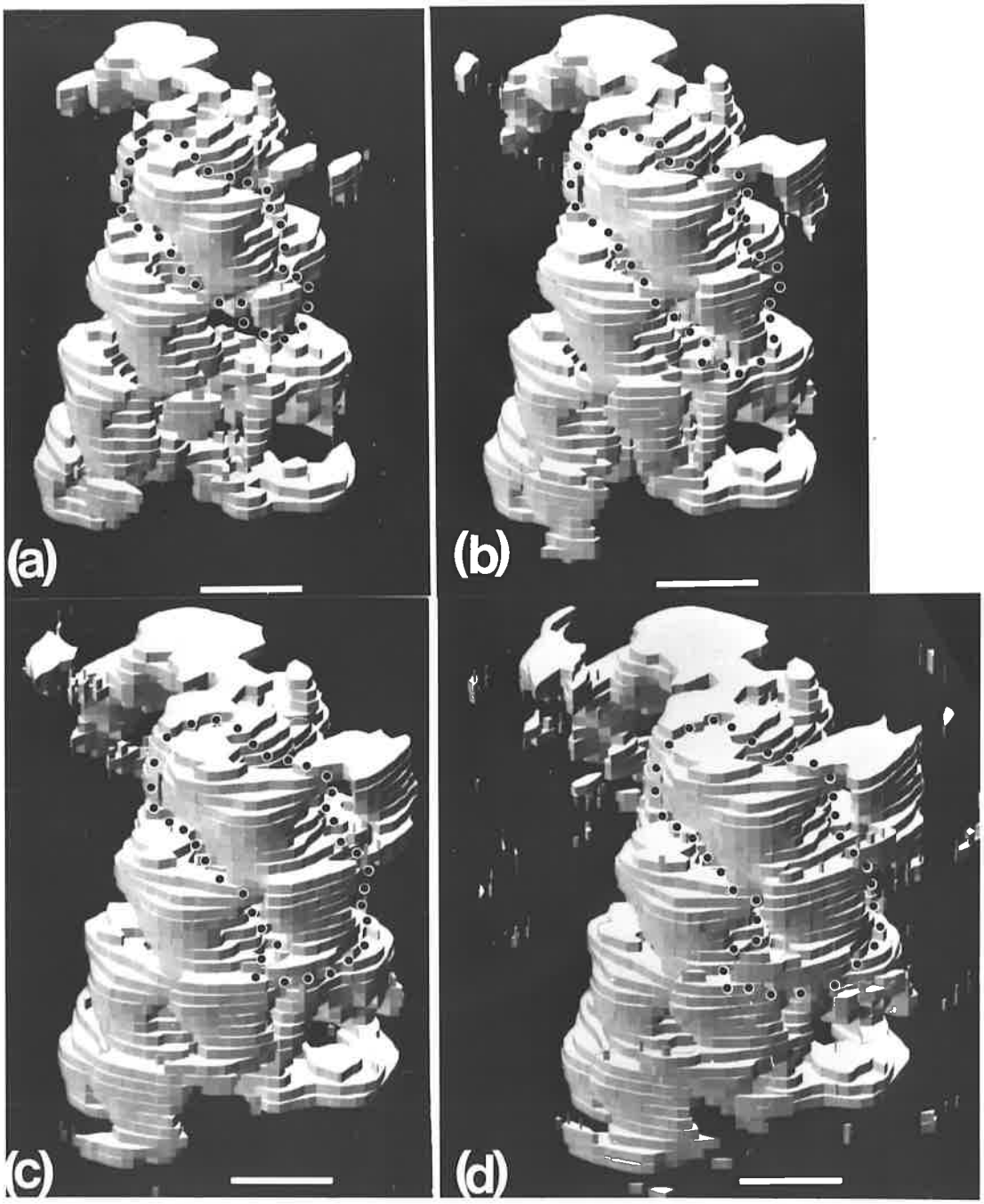

Fig. 11 The models of the reconstructed image of actin-TM-sHMM at various cut-off level generated by computer graphics. **(a)**14.8, **(b)**10.5, **(c)**7.5 and **(d)**5.5. The Bar represents 5 nm.

Fig. 12. **a**, An end-on view of the transparent model of the three-dimensional image of the actin-TM-S1 complex from Toyoshima & Wakabayashi (1985a), as the reference image.
b, An end-on view of the transparent model of the three-dimensional image of the actin-TM-sHMM complex at 10.5 cut-off level.

c, An end-on view of the transparent model of the three-dimensional image of the actin-TM-sHMM complex at 14.8 cut-off level.
d, An end-on view of the transparent model of the three-dimensional image of the actin-TM-sHMM complex at 5.5 cut-off level. Assignment of actin and S1 is according to Toyoshima & Wakabayashi (1985b) and Tomioka *et al.*(1986). Bar represents 5 nm.

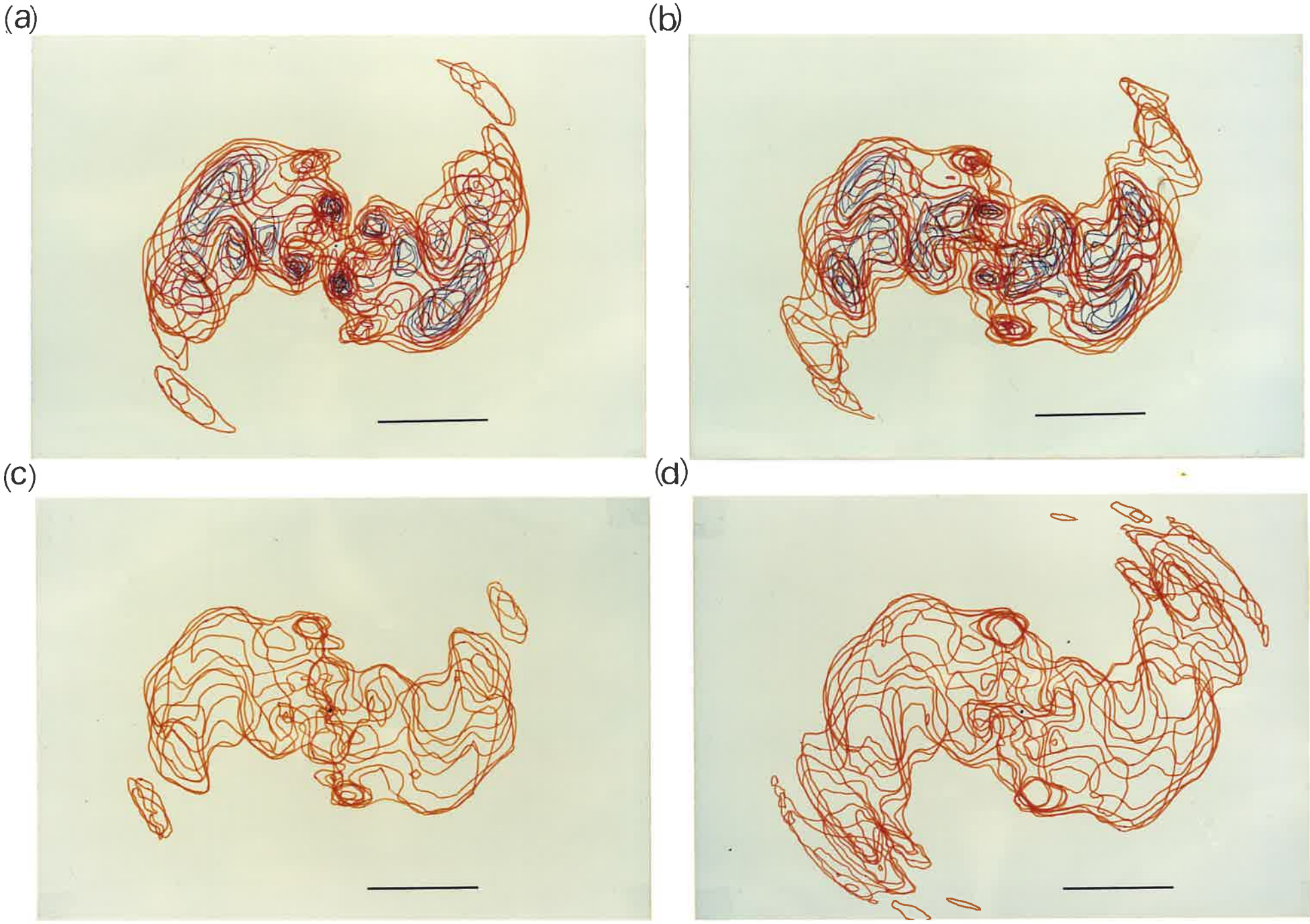

Fig.12

Fig. 13. Comparison of stain distributions of **(a)** actin-TM-sHMM complex and **(b)** actin-TM-S1 complex. A 6.67 Å × 6.0 Å × 6.0 Å cell was used in real space to sample the densities of the reconstructed images. The number of cells with a certain value of density within a cylinder of radius of 103 Å and height 360 Å was counted by computer. The dotted areas represent 82 % volume recovery for sHMM complex and 76 % for S1 complex respectively.

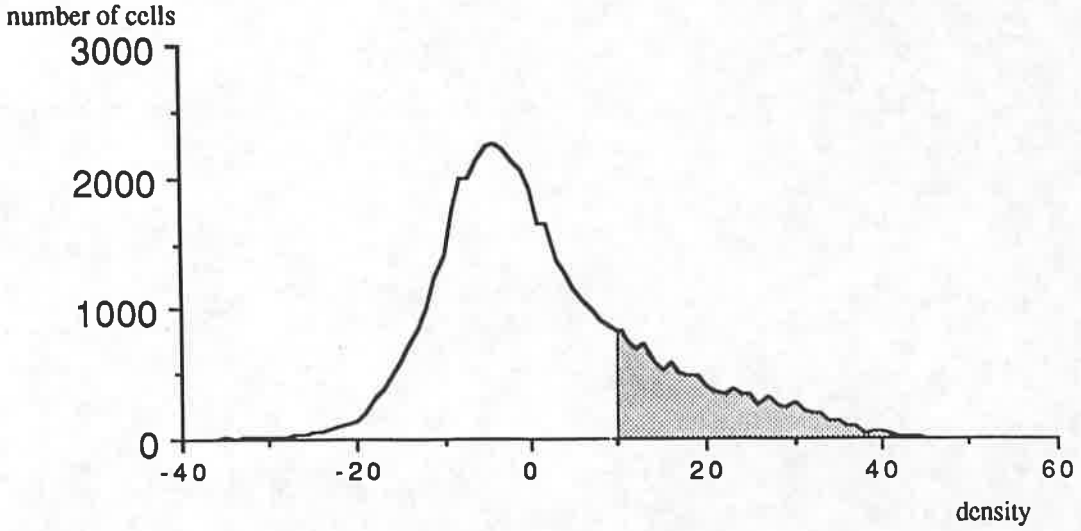

fig. 13(a).

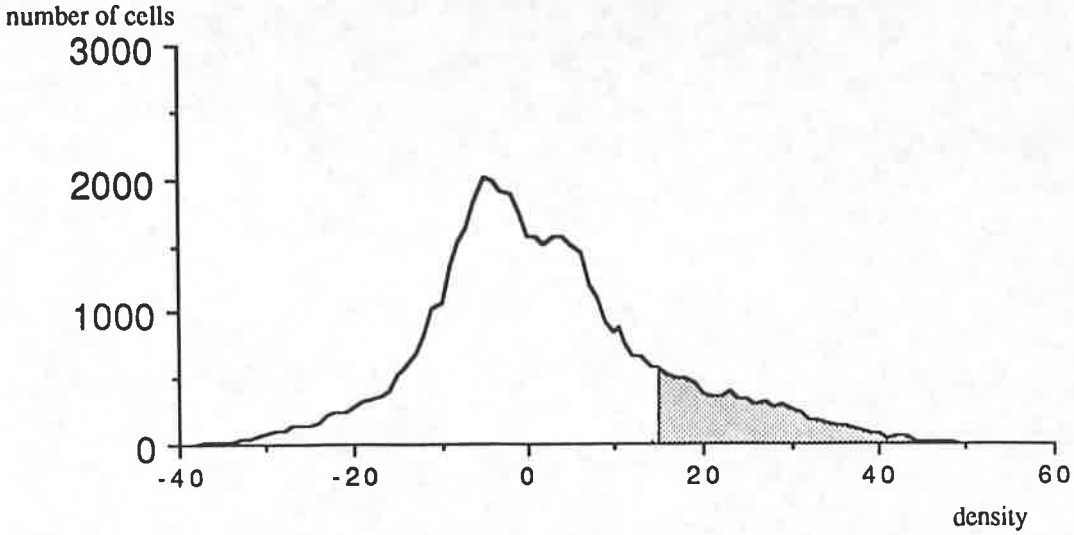

fig. 13(b).